Journal of Applied Mechanics and Technical Physics, Vol. 48, No. 3, pp. 361–367, 2007

LAMINAR–TURBULENT TRANSITION IN THE BOUNDARY LAYER ON CONES IN A HYPERSONIC FLOW AT HIGH REYNOLDS NUMBERS PER METER

A. A. Vasil'ev,[1,2] **V. N. Rychkov,**[1,2] **and M. E. Topchiyan**[1,2]

UDC 532.57; 533.6/7; 535.8; 629.7/.016

The laminar–turbulent transition is experimentally studied in boundary-layer flows on cones with a rectangular axisymmetric step in the base part of the cone and without the step. The experiments are performed in an A-1 two-step piston-driven gas-dynamic facility with adiabatic compression of the working gas with Mach numbers at the nozzle exit $\mathrm{M}_\infty = 12$–14 *and pressures in the settling chamber* $P_0 = 60$–600 MPa. *These values of parameters allow obtaining Reynolds numbers per meter near the cone surface equal to* $\mathrm{Re}_{1e} = (53\text{–}200) \cdot 10^6$ m^{-1}. *The transition occurs at Reynolds numbers* $\mathrm{Re}_{\mathrm{tr}} = (2.3\text{–}5.7) \cdot 10^6$.

Key words: *hypersonic flow, flow around a cone, laminar–turbulent transition, high Reynolds numbers.*

Introduction. The separation properties of a hypersonic boundary layer passing from the laminar to the turbulent state at junctions of various elements of flying vehicles (in inlets, flaps, etc.) are often responsible for the flow pattern around the body as a whole and its aerodynamic characteristics.

Boundary-layer stability and laminar–turbulent transition have been studied in many papers. Because of the restrictions on the paper volume, the state of the art of this problem cannot be discussed in detail (see [1–7]). Unlike [1–7], the data described below were obtained for stagnation parameters that have not yet been reproduced in a gas-dynamic experiment.

The present paper describes the result of investigations of the laminar–turbulent transition in the boundary layer on cones with and without a rectangular step. The study was performed in an A-1 piston-driven two-step gas-dynamic facility with adiabatic compression [8]. Up to now, for free-stream Mach numbers $\mathrm{M}_\infty > 10$, the range of natural (for promising hypersonic vehicles) free-stream Reynolds numbers could not be completely reproduced in experimental facilities (see, e.g., [9]), and the main source of data on the transition were in-flight results. A high pressure in the settling chamber of the A-1 facility ($P_0 \leqslant 1000$ MPa) and a rather low temperature ($T_0 = 1200$–2000 K) ensure obtaining record Reynolds numbers per meter ($\mathrm{Re}_{1\infty} = \rho_\infty v_\infty / \mu_\infty$) at the nozzle exit. Even for comparatively small model sizes, this allows one to obtain, for $\mathrm{M}_\infty = 8$–18, Reynolds numbers close to natural ones (for flight of promising hypersonic vehicles) and to observe (without artificial tripping) the boundary-layer transition from the laminar to the turbulent state at distances of the order of 30–50 mm from the tip of the model tested. The test time (20–200 msec) and the small size of the model allow one to assume the flow on all parts of the examined model to be steady and to obtain measurements at several points during one run.

The A-1 layout and its operation principle were described in detail in [8]. The facility has the following limiting parameters: pressure in the settling chamber $P_0 = 1000$ MPa, maximum stagnation temperature $T_0 =$

[1]Lavrent'ev Institute of Hydrodynamics, Siberian Division, Russian Academy of Sciences, Novosibirsk 630090; topch@hydro.nsc.ru. [2]Novosibirsk State University, Novosibirsk 630090. Translated from Prikladnaya Mekhanika i Tekhnicheskaya Fizika, Vol. 48, No. 3, pp. 76–83, May–June, 2007. Original article submitted October 10, 2006; revision submitted December 11, 2006.

2000 K, settling chamber volume $V \approx 50$ cm^3, nozzle-exit diameter $d = 8$–40 mm, Mach number at the nozzle exit $M_\infty = 7$–20, maximum Reynolds number per meter at the nozzle exit $Re_{1\infty} = 240 \cdot 10^6$ m^{-1}, test time with the maximum pressure $\tau = 0.02$–0.30 sec, working gases N_2, air, etc.

The A-1 facility has a typical gas-dynamic duct for conventional wind tunnels: a conical nozzle (with inner surface roughness less than 1 μm), test section with transparent optical walls, diffuser, and vacuum tank with a volume of 0.2 m^3 evacuated to a pressure of approximately 5 kPa. The use of nozzle inserts with throat diameters ranging from 1.0 to 0.3 mm allows obtaining flows with Mach numbers $M_\infty = 8$–18.

The present study was aimed at obtaining data on the laminar–turbulent transition of the boundary-layer flow on a cone with high values of both Mach numbers and Reynolds numbers per meter simultaneously.

Organization of Experiments. The study was performed with three models in the form of a steel cone with an apex angle of 15°. All models were set on a cylindrical holder 13 mm in diameter. The roughness of the model surface was less than 1 μm, and the rounding diameter of the model tip was 0.3 mm. The model was mounted at the center of the flow, and the model tip was inside the nozzle at a distance of 1–5 mm from the nozzle exit.

To reach the transition on small-size models, which could be tested in A-1 (for $M_\infty = 12$–14, the nozzle-exit diameter is approximately 34 mm), the first series of tests was performed with model No. 1, which had a rectangular ring-shaped flange 1.4 mm high and 4 mm wide at the cone base. The length of the generatrix was $L_0 = 48.2$ mm.

As the transition on model No. 1 was registered at a distance of 30–40 mm from the model tip, the ring-shaped flange located at the point of junction with the holder was replaced in the second series of tests by a step 0.8 mm high (model No. 2). The length of the generatrix was $L_0 = 48.5$ mm. The third (largest) series of tests was performed with model No. 3 ($L_0 = 49.3$ mm) where the conical part joined the holder without any step.

The working gas was commercial nitrogen supplied in liquid form in Dewar flasks. After evaporation in an evaporation tank, gaseous nitrogen was compressed by a compressor to 15 MPa and was stored in standard gas holders at this pressure and room temperature.

The schlieren pictures (shadowgraphs) of interaction of the hypersonic flow with the model were taken by a "Karl Zeiss" device for hairline photographing (vision field of 80 mm), in combination with a sweep camera and stroboscopic lighting. The lighting generator ensured a prescribed number of frames with a framing frequency of 75–90 Hz, the time of exposure of one frame being $0.5 \cdot 10^{-6}$ sec. The angular velocity of the sweep camera was chosen to be as low as possible, but no overlapping of frames was allowed.

The static parameters of the gas in low-pressure and high-pressure receivers were measured and the pressure transducers were calibrated by standard test indicating pressure gauges with a class of accuracy of 0.4. The working gas pressure in the settling chamber and its variations were recorded by a manganin gauge specially developed for diagnosing the working gas compressed in the settling chamber [10] and included into the active arm of a conventional bridging scheme. The pressure in facility elements was registered by quartz gauges with a specially developed structure, which were equipped by wide-band charge amplifiers with a low-resistance output. The signals from the gauges were recorded by an N-115 mirror-galvanometer oscillograph.

Figure 1 shows the pressure oscillograms. [In this experiment, the maximum value of $P_0(t)$ was 395 MPa.] The numbers 1–9 indicate the time instants: the signals of the photodiode recording the stroboscope flashes, which correspond to the numbers of the frames.

The first increase in pressure in the settling chamber corresponds to adiabatic compression of the working gas by the heavy piston of the first stage of the facility. After automatic initiation of the second stage, the working gas is additionally compressed by the piston of the pressure multiplier to a necessary maximum pressure and then is displaced from the settling chamber. Though the throat diameter was sufficiently large for such a settling chamber (for this reason, the pressure multiplier "did not have enough time" to follow gas exhaustion), the pressure during the time interval between frames 5 and 7 was sustained constant within ±5% owing to compression. Therefore, the exhaustion may be considered as quasi-steady at each time instant of photographing and corresponding to the pressure measured in the settling chamber. The pressure oscillogram P_m refers to the pressure on the pressure multiplier of the second stage. When the plunger meets the settling chamber wall, a jump of the pressure P_m is recorded, which coincides in time with a drastic decrease in the pressure P_0.

Nozzle startup occurs already at the stage of gas compression in the first stage, as soon as the critical pressure is reached in the settling chamber, and the gas escapes to the test section of the gas-dynamic duct of the facility.

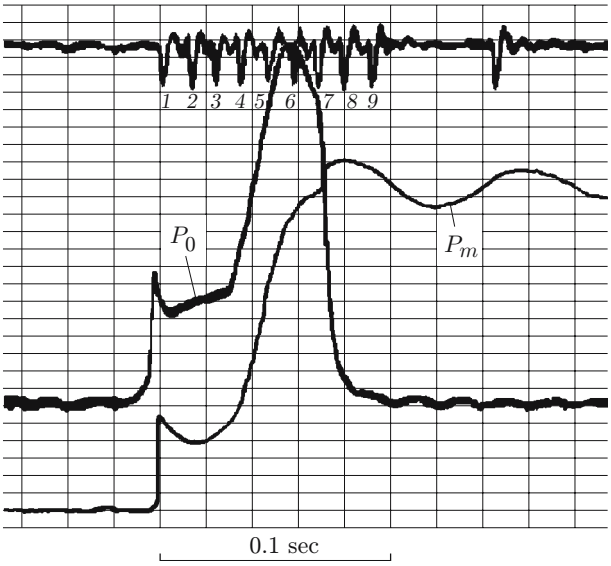

Fig. 1. Pressure oscillograms in the settling chamber P_0 and in the pressure multiplier P_m: the times instants of photographing are marked by 1–9.

In the present series of experiments, the hypersonic flow was obtained in a conical nozzle with a throat diameter $d_* = 0.805$ mm, nozzle angle of 8°, and exit diameter of 34 mm. The gas and model temperatures at the beginning of the test were equal to room temperature, which varied within $T_{00} = 288$–294 K.

As the measurements performed in [11] showed that the heat losses toward the walls may be neglected for the goals of the present work, the current parameters of the flow at the nozzle exit (static temperature T_∞, pressure P_∞, and Reynolds number $\mathrm{Re}_{1\infty}$) for all time instants (frames) were calculated on the basis of the measured initial parameters P_{00}, T_{00}, and $P_0(t)$ with the model of adiabatic compression and expansion of the gas. For the same reason and by virtue of the short test time (30–60 msec for $d_* = 0.805$ mm), the model-surface temperature T_w may be assumed to be equal to room temperature T_{00}, and its effect on the boundary layer may be neglected. The calculations were performed by formulas derived in [12] and a special code developed by the authors of the present paper.

Results of Studying the Boundary-Layer Transition. Figure 2 shows the typical frames of the Schlieren pictures around the model. The Foucault knife of the optical system was mounted horizontally. Zones of a purely laminar flow, laminar–turbulent transition, and accelerated increase in thickness of the turbulent boundary layer can be distinguished. An analysis of the flow patterns suggests that an increase in pressure in the settling chamber shifts the beginning of the laminar–turbulent transition zone toward the model tip [cf. consecutive frames of one test (Figs. 2c and 2d)]. The beginning of the transition zone was determined as the point with a jump (inflection) of density caused by boundary-layer turbulization [13].

For frames in Fig. 2, the calculated pressure at the nozzle exit was $P_\infty = 7$–27 mm Hg, whereas the pressure in the test section at the beginning of exhaustion was $P_\infty = 20$–40 mm Hg. Oblique shock waves arising at the nozzle edge owing to jet overexpansion obviously cross the boundary layer downstream of the transition beginning. The pressure generated by these shock waves and calculated by the angle of their inclination is equal to or lower than the pressure behind the bow shock wave; hence, these shock waves did not affect the transition in our experiments.

At high pressures in the settling chamber, owing to real gas effects and to the fact that the working gas in the A-1 facility is obtained by adiabatic compression, the stagnation temperature and the flow Mach numbers at the nozzle exit M_∞ and above the model surface M_e depend on the pressure in the settling chamber. Figure 3 shows the Mach numbers and the Reynolds number per meter $\mathrm{Re}_{1\infty}$ at the nozzle exit as functions of pressure. A small scatter in the values of M_∞ and $\mathrm{Re}_{1\infty}$ can be attributed to variations of the initial (room) temperature of the working gas and to the error in measuring the initial and current pressures; for M_e, another reason is the error in measuring the angles of inclination of the bow shock wave to the flow. It follows from Fig. 3 that the values reached in the experiments were $\mathrm{M}_\infty = 12$–14, as was calculated by the above-mentioned code with allowance for real gas effects and boundary-layer displacement thickness.

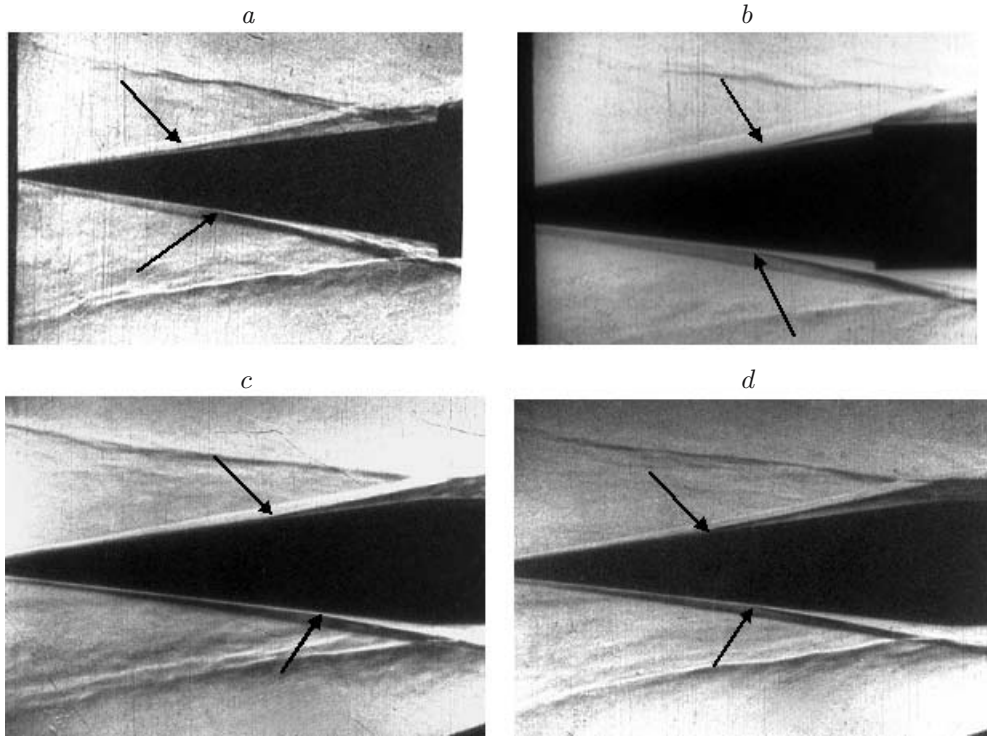

Fig. 2. Flow pattern around the cone: (a) $P_0 = 348.5$ MPa and a step 1.4 mm high; (b) $P_0 = 201.5$ MPa and a step 0.8 mm high; (c) $P_0 = 459.0$ MPa and no step; (d) $P_0 = 589.7$ MPa and no step; the arrows indicate the beginning of the transition zone.

Above the model surface, the Mach numbers $\mathrm{M}_e = 8.5$–10, Reynolds numbers Re_{1e}, density ρ_e, velocity v_e, and viscosity of the medium μ_e were calculated on the basis of the experimentally determined angles of inclination of the bow shock wave toward the flow φ and the cone apex angle β with the use of formulas for an inviscid flow around the cone derived in [14–16]. By introducing the dimensionless flow velocity η as the ratio of velocity to its maximum possible value, the dimensionless temperature as the ratio of temperature to its free-stream value ($\theta = T/T_\infty$), and the degree of compression in the shock wave $\sigma = \rho/\rho_\infty$, we can express the Reynolds number per meter on the cone surface Re_{1e} via Re_1 if the ratio of specific heats is $c_p/c_v = 1.4$:

$$\mathrm{Re}_{1e} = \mathrm{Re}_1 \eta_e \sigma_e / \theta_e.$$

Here

$$\eta_e = \eta_\infty \frac{\cos\varphi}{\cos^2(\varphi - \beta)}; \qquad \sigma_e = \Big(\frac{1-\eta_e^2}{1-\eta_\infty^2}\Big)^{2.5} \frac{167\mathrm{M}_{\infty n}^7}{(7\mathrm{M}_{\infty n}^2 - 1)^{2.5}(1 + 0.2\mathrm{M}_{\infty n}^2)^{3.5}}$$

[$\mathrm{M}_{\infty n} = \mathrm{M}_\infty \sin\varphi$ and $\theta_e = (1-\eta_e^2)(1 + 0.2\mathrm{M}_\infty^2)$]. The Mach number above the cone surface was determined by the relation $\mathrm{M}_e = \mathrm{M}_\infty \eta_e / \sqrt{\theta_e}$.

The length L_{tr} in the expression for $\mathrm{Re}_{\mathrm{tr}}$ ($\mathrm{Re}_{\mathrm{tr}} = \mathrm{Re}_{1e} L_{\mathrm{tr}}$) was counted along the cone generatrix from the model tip to the beginning of the laminar–turbulent transition zone determined from the photographs. The error of measurement of L_{tr} was approximately 3%. The real angle of attack was determined with allowance for the correction.

The pressure of nitrogen $P_0(t)$ in the settling chamber at the time instants of photographing was determined from oscillograms similar to those shown in Fig. 1; in the present series of tests, it varied from 63 to 570 MPa with an error smaller than 2%. The temperature $T_0(t)$ was determined by calculations and varied within 935–1610 K.

The Reynolds number per meter at the nozzle exit $\mathrm{Re}_{1\infty}$ was $(40\text{–}120) \cdot 10^6$ m^{-1}; the Reynolds number per meter behind the bow shock wave above the model surface was $\mathrm{Re}_{1e} = (\rho v/\mu)_e = (50\text{–}200) \cdot 10^6$ m^{-1}.

Figure 4 shows the Reynolds numbers per meter behind the shock wave above the model surface Re_{1e} and the distances L_{tr} between the model tip and the transition point as functions of the pressure in the settling chamber.

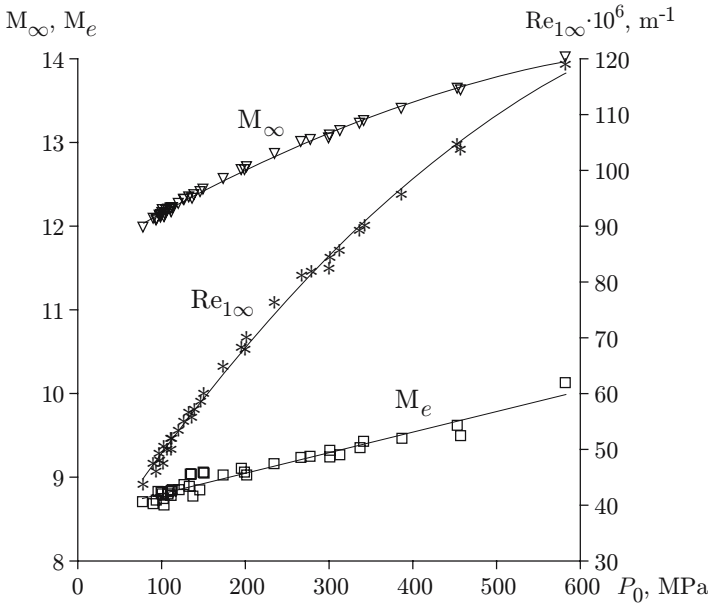

Fig. 3. Dependences of M_∞, M_e, and $Re_{1\infty}$ on pressure in the settling chamber.

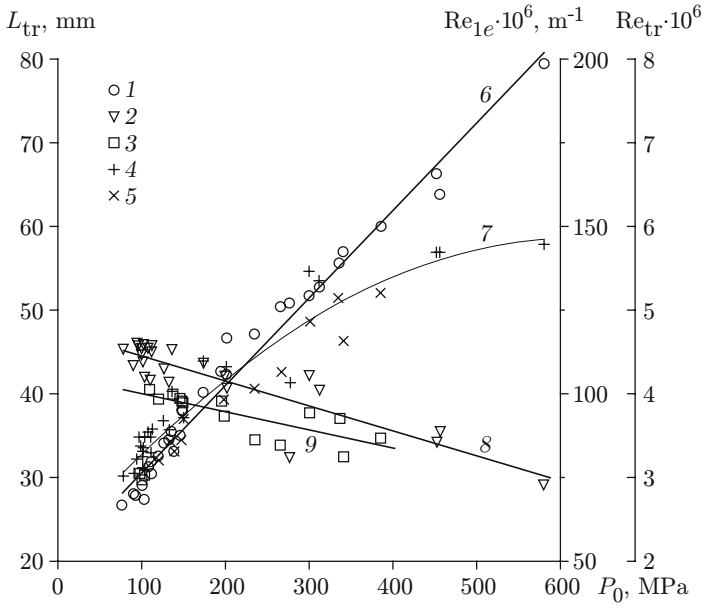

Fig. 4. Length of transition L_{tr} and Reynolds numbers versus pressure: points 1–5 are the experimental data: 1) Re_{1e}; 2) L_{tr} on the cone without the step; 3) L_{tr} on the cone with the step; 4) Re_{tr} on the cone without the step; 5) Re_{tr} on the cone with the step; curves 6–9 are the approximations by formula (3) (curve 6), formula (4) (curve 7), formula (1) (curve 8), and formula (2) (curve 9).

It should be noted that the values of L_{tr} for models without the step are higher than those for models with the step. The corresponding experimental values are located close to the straight lines plotted by the least squares technique:

$$L_{tr} = (47.4 - 2.85 \cdot 10^{-2} P_0); \tag{1}$$

$$L_{tr} = (42.3 - 2.26 \cdot 10^{-2} P_0), \tag{2}$$

i.e., the presence of the step leads to a significant decrease in L_{tr}. [In Eqs. (1) and (2), and further, P_0 is measured in megapascals, L_{tr} in millimeters, and Re_{e1} in m^{-1}.]

The dependence $\mathrm{Re}_{e1}(P_0)$ is adequately approximated by the straight line

$$\mathrm{Re}_{e1} = (49.9 + 0.256P_0) \cdot 10^6. \tag{3}$$

Figure 4 displays a substantial scatter in the values of the transition Reynolds number $\mathrm{Re}_{\mathrm{tr}}$ calculated on the basis of Re_{1e} and the distance L_{tr} for models without and with the step. The points are seen to be divided into two families. The solid curve (7) is the general law described (for all points, with a standard deviation of $0.24 \cdot 10^6$) by the least squares technique by the empirical formula

$$\mathrm{Re}_{\mathrm{tr}} = (2.163 + 1.169 \cdot 10^{-2}P_0 - 9.415 \cdot 10^{-6}P_0^2) \cdot 10^6. \tag{4}$$

A comparison of the data obtained with available results on the boundary-layer flow transition [1–4, 6] shows that, with an increase in pressure in the settling chamber, an increase in Reynolds numbers per meter Re_{1e} leads to a monotonic (though slowing down) increase in the Reynolds numbers $\mathrm{Re}_{\mathrm{tr}}$ corresponding to the beginning of the transition. Thereby, the values of L_{tr} decrease, and the transition zone is shifted toward the model tip. This effect was noted, e.g., in [1, 2], but it was observed at Mach numbers M = 2–4 and in a different range of Reynolds numbers per meter Re_{1e} (up to $74 \cdot 10^6$ m^{-1}).

It should be noted that the transition Reynolds numbers obtained in this work are lower than those in other papers. A possible reason is the difference in test techniques. Pressure or heat-flux measurements are usually performed. Thus, the results obtained in the present work, apparently, refer to the beginning of the transition.

Conclusions. The process considered is a sophisticated phenomenon affected by many factors; therefore, the results described are typical of this facility and particular conditions of the flow. Nevertheless, these experiments with appropriate Mach numbers reproduced Reynolds numbers typical of promising hypersonic flying vehicles. Therefore, the study in this field will be continued, in particular, the range of pressures in the settling chamber will be expanded to 800–900 MPa to obtain the values of $\mathrm{Re}_{1\infty}$ at a level of $240 \cdot 10^6$ m^{-1}, and similar experiments will be performed with other models at higher Mach numbers.

The authors are grateful to A. M. Kharitonov for his useful advice and comments in discussions of the results obtained.

Part of this work was performed within the framework of the Foundation "Leading Scientific Schools of Russian Federation," Program "Mechanics of Shock Waves and Detonation Processes" (Grant No. NSh-8583.2006.1).

REFERENCES

1. V. V. Struminskii, A. M. Kharitonov, and V. V. Chernykh, "Experimental study of the laminar to the turbulent boundary layer at supersonic velocities," *Izv. Akad. Nauk SSSR, Mekh. Zhidk. Gaza*, No. 2, 30–34 (1972).
2. V. G. Pridanov, A. M. Kharitonov, and V. V. Chernykh, "Combined effect of Mach and Reynolds numbers on the boundary-layer transition," *Izv. Akad. Nauk SSSR, Mekh. Zhidk. Gaza*, No. 1, 160–163 (1974).
3. S. A. Gaponov and A. A. Maslov, *Development of Disturbances in Compressible Flows* [in Russian], Nauka, Novosibirsk (1980).
4. B. V. Boshenyatov, V. V. Zatoloka, and M. I. Yaroslavtsev, "Separated flow around cones with a turbulent boundary layer at Mach numbers 8, 3, and 10," *Izv. Sib. Otd. Akad. Nauk SSSR, Ser. Tekh. Nauk*, No. 8, Issue 2, 43–50 (1975).
5. Yu. P. Goonko, V. I. Zvegintsev, I. I. Mazhul, et al., "Wind-tunnel testing of a hypersonic scramjet model at high Mach and Reynolds numbers," *Teplofiz. Aéromekh.*, **10**, No. 3, 321–345 (2003).
6. A. A. Maslov, A. N. Shipluk, D. A. Bountin, and A. A. Sidorenko, "Mach 6 boundary-layer stability experiments on sharp and blunted cones," *J. Spacecraft Rockets*, **43**, No. 1, 71–76 (2006).
7. E. Reshotko, "Boundary layer instability, transition and control," AIAA Paper No. 94-0001 (1994).
8. V. N. Rychkov, M. E. Topchiyan, A. A. Meshcheryakov, and V. I. Pinakov, "Use of high pressures for solving problems of hypersonic aerodynamics," *J. Appl. Mech. Tech. Phys.*, **41**, No. 5, 855–864 (2000).
9. M. E. Topchian and A. M. Kharitonov, "Wind tunnels for hypersonic study," *Thermophys. Aéromech.*, **1**, No. 1, 89–103 (1994).
10. V. N. Rychkov, "Method of measuring pressures up to 1 GPa on a pulsed gas-dynamic device," *J. Appl. Mech. Tech. Phys.*, **39**, No. 5, 816–820 (1998).

11. V. N. Rychkov, "Possibilities of simulating aerogasdynamic processes on a pulsed adiabatic facility with superhigh pressure," Candidate's Dissertation in Phys.-Math. Sci., Novosibirsk (1995).
12. N. A. Zykov and R. M. Sevast'yanov, "Materials on calculation of gas-dynamic facilities with high stagnation parameters of nitrogen," *Tr. TsAGI*, No. 1329 (1971).
13. W. Merzkirch, *Flow Visualization*, Academic Press, New York (1974).
14. G. N. Abramovich, *Applied Gas Dynamics* [in Russian], Nauka, Moscow (1976).
15. N. F. Krasnov, *Applied Aerodynamics* [in Russian], Vysshaya Shkola, Moscow (1974).
16. R. M. Sevast'yanov, "Approximate calculation of a hypersonic flow of a chemically reacting gas around a cone," *Tr. TsAGI*, No. 1086 (1967).